BI-DIRECTIONAL CYCLIC LOADING EXPERIMENT ON A 3-D BEAM-COLUMN JOINT DESIGNED FOR DAMAGE AVOIDANCE

Luoman Li[1], John B Mander[2], Rajesh P Dhakal[3]

Abstract

A near full-scale 3D jointed precast prestressed concrete beam to column connection designed and constructed in accordance with an emerging *Damage Avoidance Design* (DAD) philosophy is tested under displacement controlled quasi-static reverse cyclic loading. The performance of the subassembly is assessed under unidirectional loading along both orthogonal directions as well as under concurrent bi-directional loading. The specimen is shown to perform well up to 4% column drift with only some minor flexural cracking in the precast beams, while the precast column remains uncracked and damage-free. This superior performance is attributed to steel armoring of the beam-ends to mitigate the potential for concrete crushing. Under bi-directional loading a tapered shear-key layout is used to effectively protect the beams against adverse torsional movements. A three-phase force-displacement relationship is proposed which gives due consideration to: the pre-rocking flexural deformation of the beam; the rigid body kinematics during the rocking phase; and the yielding of the external dissipaters and post-tensioning tendons. Good agreement between the proposed theoretical model and experimental observation is demonstrated. An equivalent viscous damping model is also proposed to represent both change in the prestress force in the subassembly and yielding of the supplemental energy dissipaters in the rocking connection.

Introduction

Capacity design for monolithic reinforced concrete structures aims to ensure adequate ductility by enforcing all inelastic deformation to develop in well-detailed regions, known as plastic hinge zones. Such regions can sustain large rotations despite undergoing severe damage. Since the majority of inelastic rotations are expected to be accommodated at designated plastic hinge zones within the structure, the remaining structural components are safely protected during large earthquakes. Recent earthquakes such as the 1994 Northridge and 1995 Kobe events have confirmed the adequacy of capacity design techniques in preventing structural collapse and thereby ensuring life-safety, which is a primary objective of seismic design. But, these earthquakes have also highlighted the extensive damage levels that can be expected in capacity-designed ductile structures during earthquakes. As a consequence, significant economic losses may be incurred due to damage, down-time and even death/injury. There is now a greater awareness and demand from clients and the public for engineers to provide structural systems where damage is minimized or avoided while preservation of life-safety is maintained. Jointed rocking structures have shown promise of fulfilling this dual objective.

In jointed precast construction which is known to be significantly faster than the traditional monolithic construction, precast seismic beams are dropped between columns and are supported by shear keys. Prestress is fed through the frame, and after all precast beams

[1] Research Assistant, Department of Civil and Natural Resources Engineering, University of Canterbury, Christchurch, New Zealand
[2] Zachry Professor of Design and Construction Integration I, Zachry Department of Civil Engineering, Texas A&M University, College Station, TX 77843-3136
[3] Senior Lecturer, Department of Civil and Natural Resources Engineering, University of Canterbury, Christchurch, New Zealand

are in place they are post-tensioned. One of the critical issues with such jointed construction is to ensure that every beam-to-column connection must be fully engaged after the post tensioning is applied. One possible solution for this strict tolerance requirement is to provide a cast-in-situ end for each beam where steel armor plates and small number of stirrups are installed and cast on site. In this way any length variation in the manufactured precast beams can also be accommodated. The strength of such connection can be improved and cracking in the cast-in-situ zone can also be controlled by using high strength concrete.

Previous investigations on jointed precast frame systems (MacRae and Priestley 1994, Stone et. al. 1995, Priestley et. al. 1999) have demonstrated that such frames possess certain seismic performance advantages over traditionally designed ductile systems. It has been found that in the jointed precast frame, large nonlinear deformations are accommodated via gap opening and closing at the interface between the precast elements. Due to the action of unbonded prestress, a significant reduction in damage over conventional reinforced concrete systems is expected. Furthermore, the re-centering effect provided by the unbonded prestress allows a jointed precast frame system to return to its undeformed shape with negligible residual displacement upon removal of the lateral loads.

Mander and Cheng (1997) proposed a *Damage Avoidance Design* (DAD) philosophy for bridge piers whereby armoring of column ends is introduced to further mitigate any damage potential. Recently, Davies (2004) and Arnold (2004) applied these DAD principles (i.e. armoring of beam ends) to precast concrete beam-to-column connections. They experimentally demonstrated through numerous tests that with appropriate steel-to-steel armoring at the beam-to-column interface, damage under large seismic displacements could be avoided. However, their armoring details required an extensive amount of welding in order to fabricate the steel caps for the precast-ends.

This paper presents the results of an experimental study where simple armoring details are implemented at the connection interfaces. Unlike previous unidirectional tests, experiments are conducted using bi-directional lateral loading as a means of assessing more realistically the damage avoidance potential of jointed and armored precast concrete frame systems under earthquake loading.

Design and construction of the test specimen

An 80% scaled beam-to-column joint sub-assemblage was designed and constructed as shown in Figure 1. The test specimen represents a jointed precast beam-to-column connection abstracted from one of the lower storeys of a typical New Zealand office building (Figure 1 (b)). The structural design of the prototype jointed precast system was loosely based on the well known “Red book” ten storey building example (Bull and Brunsdon 1998) that applies the provisions of the New Zealand concrete design standard (NZS3101:1995). As depicted in Figure 1 (a), the prototype building consists of two-way moment resisting frames: a jointed precast seismic frame in one direction and a jointed precast gravity frame in the orthogonal direction. The concrete floor is assumed to be a one-way precast flooring system such as hollow-core units or double tees. The building is located in Christchurch, New Zealand where an intermediate soil is assumed in the design calculations. Gravity loads assumed in the design calculations are: 3.5kPa floor load, 0.75kPa superimposed dead load and probable live load of 0.65kPa.

As outlined in Figure 1 (b), the 3-dimensional beam-column joint subassembly consists of two seismic half-beams and one gravity half-beam in the orthogonal direction. Specimen dimensions and reinforcing detailing for the physical model are shown in Figure 1 (c, d and e). The specimen consists of 700mm square column, and 400mm wide by 560mm deep beam segments in both orthogonal and transverse directions. The length of beams and column segment in the subassembly are 4m and 3.2m respectively (this assumes the point of

inflection is at mid-span of the beams and mid-height of the column). The nominal moment capacity of the rocking joint in the subassembly was designed to be 500kN-m; similar to that of the hinge region in the 80%-scaled ductile frame of the prototype building. The main resistance was provided by two 26.5mm diameter high-strength high-alloy prestressing thread-bars (Dywidag^{TM}) (f_y = 1100MPa) in the test subassembly. All three precast beams were designed assuming a concrete compressive strength of f'_c = 45MPa.

To protect the concrete from damage during rocking, the ends of the precast beams that join at the column face were armored. Steel angles (100mm x 100mm x 12mm) were placed at the top and bottom corners of the beam. At one beam end, an adjustable cast-in-situ wet joint was implemented, while the other beam ends were precast dry joints. By providing an adjustable beam-end at several intervals along the frame allows tolerances in precast beam length to be accommodated during construction.

A cracked elastic design was employed to detail the longitudinal reinforcement in the precast beam segments. In this design approach, a sufficient quantity of mild steel was provided to ensure that yield of the longitudinal reinforcing was prevented, while the concrete compressive stresses were kept below 70 percent of the 28 day strength (f'_c). This ensured the precast beam elements remained essentially elastic even when the connection reached its calculated over-strength capacity. Shear design of the precast beam elements followed the New Zealand Concrete Standard (NZS3101:1995). With a total initial axial load of 400kN provided by the two prestressing thread-bars, the required transverse reinforcement was less than for a conventional system; thus a maximum allowable stirrup spacing of 250mm was used in the central region of each beam. Closely spaced (100mm centre-to-centre) stirrups were placed at beam ends to help transfer the large bursting forces arising from the post-tensioned prestress together with the rocking action of the connection.

The 700mm square precast concrete column was post-tensioned by four unbonded 32mm diameter (Macalloy^{TM}) high strength thread-bars to simulate the level of axial load ($0.1f'_cA_g$) that would be expected on the lower storey of the office building. The column had a measured 28 day concrete compressive strength of f'_c = 58MPa. Three 400mm wide by 560mm long by 20mm thick mild steel plates were cast at column faces where the precast beams met with the column face.

Only minimum longitudinal steel (ρ_l = 0.008) was provided in the column, which consisted of 12 high-strength (f_y = 500MPa) 20mm diameter threaded reinforcing bars (Reidbar^{TM}). Such a low reinforcement ratio prevents congestion of reinforcement in the joint region and therefore minimizes construction difficulties; the required strength was largely provided by the longitudinal prestress effect. Moreover, due to the high axial load (2000kN) provided by the vertical tendons, only a minimum amount of transverse shear hoops were needed. Thus, high-strength plain round bars HR12 (with f_y = 500MPa) were used as hoop-sets at 200mm centers to resist the most adverse shear force generated in the column.

Five double HR12 hoop-sets with a center-to-center spacing of 100mm were placed in the joint region to assist in the transfer of the large design shear forces through the joint. At both ends of the column, 4 hoop-sets at 100mm centers were used to resist the prestress bursting forces into the column. To prevent concrete from crushing, the concrete stress behind steel plate was limited to $0.7f'_c$. Based on an assumed 45 degree force redistribution angle through the plate, a 20mm thick steel plate was adopted.

As depicted in Figure 1 (c) and (e), the three precast half-beams were joined to the column through two threaded fuse “bolt-bars” via couplers cast within the beams. Except for the straight tendon in the gravity beam, the couplers used in all other tendons were bent to accommodate the change in slope. In the seismic frame (East-West) direction, the two unbonded post-tensioned prestressing thread-bars were placed parallel to the beam’s neutral

axis, while in the gravity frame (North-South) direction, a draped tendon was used in addition to a straight tendon. The mid section of the threaded fuse "bolt-bar" was machined down to form the weakest link within the joint to protect the main prestressing thread-bars within the beam in a large or "near-field" earthquake event. These fuse bolt-bars also provide some additional amount of energy dissipation when they yield.

Supplementary energy dissipaters in the form of mechanically machined mild steel rods were installed externally across the beam-to-column connection. Along the seismic loading direction one dissipater was installed at mid-height across the connection in each side of the beam while in the gravity loading direction two dissipaters were installed across the connection at the top and bottom of the gravity beam, respectively. Tapered shear key studs were installed on the face of the column across the connections to provide torsional resistance during bi-directional loading. The shear keys were also designed to carry the weight of the beam and provided temporary support for the beams during construction.

Experimental set-up, instrumentation and testing procedures

Figure 2 presents details of the experimental setup. Two large hydraulic actuators, one along the East-West direction (Ram A) and the other along North-South direction (Ram B), were installed across the reaction frames on top of the column. A third hydraulic actuator (Ram C) was also installed along the East-West direction at end of the gravity beam to keep the specimen movement in-plane and to avoid twisting during testing. Ram C also provided a means of measuring the amount of torsional resistance in the specimen (if any) during bi-directional testing. Movement of Ram C was synchronized to move in the same direction as Ram A but with only half of the stroke of Ram A.

Additional vertical load was applied on top of the gravity beam to simulate gravity effects through a 300kN capacity hydraulic jack on top of the gravity beam. A steel plate with a ball bearing joint on top of the hydraulic jack was bolted down to a universal support fixed on the strong floor through four threaded rods. As can be seen in the setup photograph shown in Figure 2 (d), a 1500mm long and 200mm deep by 400mm wide timber beam was used to uniformly spread the "gravity" load along the beam.

A total of 12 load cells were used to measure strut forces at beam ends, force in the hydraulic rams, and prestressing force in the high strength thread-bar tendons. Three linear potentiometers with 50mm stroke were installed along each face of the three rocking connections to monitor the connection opening and closing (Figure 2 (b) and (c)). Two 100mm linear potentiometers were installed beneath each precast beam near their rocking connection to capture the vertical movements. Eight string potentiometers were placed in various locations around the specimen to capture any out-of-plane movement (Figure 2 (b) and (c)). Strain gauges with 5mm gauge length were used to monitor longitudinal strains in the fuse bolt-bars. Two 5mm gauges were attached on the surface of each threaded fuse rod used as the energy dissipaters.

Utilizing the advantage of damage avoidance design, a single specimen was loaded several times to assess different levels of performances (Bradley et al 2008). First, unidirectional tests were carried out separately in seismic-frame (East-West) and gravity-frame (North-South) directions. In these displacement-controlled unidirectional tests, gradually increasing reversed cyclic displacements in the form of sine waves were applied to the specimen. The displacement cycles had drift amplitudes of ±0.25%, ±0.5%, ±1%, ±2%, ±3%, and two repeated cycles of the same drift amplitude were applied before increasing the drift to the next level. Thereafter, to study the behavior of the subassembly under concurrent bi-directional lateral loading, two different types of bi-axial loading paths were used namely: (i) cosine-based four-leaf clover pattern given by $x = aCos(2\theta)Cos(\theta)$ and

$y = aCos(2\theta)Sin(\theta)$; and (ii) sine-based four-leaf clover pattern given by $x = aSin(2\theta)Cos(\theta)$ and $y = aSin(2\theta)Sin(\theta)$, where a = displacement amplitude and θ = angles in radians between the load path and the x-axis. Similar to the unidirectional tests, the bi-directional test started with a radial column drift of 0.25%, which increased gradually to 4% radial drift. To separate the effect of prestressing tendons and the energy dissipaters, the specimen was tested twice; without and with the external energy dissipaters. Note that in such sequential loading tests using a single specimen, damage occurred in one test will influence the specimen's behavior in the next test. As the yielded energy dissipaters (if any) were changed and the prestressing tendons were re-stressed after each test, the only damage carried forward was the concrete cracking near the rocking interface. As preparing multiple virgin specimens for the different loading series is too costly, this minor compromise was accepted.

Theoretical modeling of lateral load vs. drift behavior

The envelop curve of lateral load vs. drift response of a jointed unbonded post-tensioned beam-to-column connection with and without supplemental energy dissipaters can be represented by a tri-linear response model. The uppermost heavy solid line in Figure 3 (a) and (b) represents the monotonic loading curve of such a system. First, the system behaves in an elastic fashion where deformation arises primarily from flexure in the prestressed concrete elements. This continues until the joint opens when the applied moment equals the combined resistance provided by the prestress and the dissipaters (if any). Joint opening is primarily a function of the level of prestress after losses. Following joint opening, the prestressing tendons elastically elongate and the dissipaters engage. Because the dissipaters are stiff due to their shortness in length, they may be assumed to yield at the initiation of joint opening. The tendons continue to elongate until they finally reach their yield capacity, following which the system is entirely plastic. It is worth noting that a small amount of energy is dissipated due to the variation of the prestress force level (δF) generated by the friction within the beam column connection.

The aforementioned lateral force vs. drift behavior can be conveniently modeled with the use of a compound form of the Menegotto-Pinto (1973) equation as follows:

$$F = \frac{(K_2 - K_1)\theta}{\left(1 + \left|\frac{K_1\theta}{F_p + F_D \operatorname{sgn}(\dot{\theta})}\right|^5\right)^{0.2}} + \frac{K_2\theta}{\left(1 + \left|\frac{K_2\theta}{F_y + F_D \operatorname{sgn}(\dot{\theta}) - (F_p + F_D \operatorname{sgn}(\dot{\theta})(1 - K_2/K_1))}\right|^{20}\right)^{0.05}} \quad \textbf{(1)}$$

where K_1 = structural stiffness prior to gap opening; K_2 = stiffness arising from the prestress effect; F_p = lateral resistance of subassembly from prestress alone; F_D = lateral resistance of the subassembly from metallic dissipaters alone; F_y = yield strength of the subassembly with prestressing only; and θ = drift angle of the column. Note that when $\dot{\theta} > 0$, $\operatorname{sgn}\dot{\theta} = 1$; and when $\dot{\theta} < 0$, $\operatorname{sgn}\dot{\theta} = -1$. Note that the powers in the denominator of the first and second parts of Equation (1) represent the degree of curvature that joins the two tangents, with higher numbers giving sharper curves. These powers (5, 0.2 and 20, 0.05) have been chosen to suit the general experimental outcomes described later.

By applying moment-area theorems, the initial system stiffness for the present sub-assemblage, K_1, can be derived as:

$$K_1 = \frac{12(EI^*_{beam})/L_b^3}{\left(\frac{L_{col}}{L}\right)^2 + \left(\frac{L_{col}-D}{L_b}\right)^3\left(\frac{EI^*_{beam}}{EI^*_{col}}\right)} \quad \textbf{(2)}$$

where EI^*_{beam} and EI^*_{col} are effective beam and column rigidity; L_b = precast beam length; L = clear span between column centre lines; L_{col} = column height; and D = beam depth.

Following gap opening, the second stiffness K_2 is given by:

$$K_2 = \left(\frac{L}{L_b}\right)^2\left(\frac{D}{L_{col}}\right)^2 \frac{K_{bolt}K_{ps}}{K_{bolt}+K_{ps}} \quad \textbf{(3)}$$

in which $K_{bolt} = A_{bolt}E_{ps}/l_{bolt}$ is the stiffness of the bolt (fuse) bar, where A_{bolt} = area and l_{bolt} = length of the fuse portion of the bolt bar. Similarly in Equation (3), $K_{ps} = A_{ps}E_{ps}/l_{ps}$ is the stiffness of the prestressing tendon in the precast beam, where E_{ps} = Young's modulus; A_{ps} = cross-sectional area, and l_{ps} = length of the prestressing tendon in the beam.

The lateral load resistance of the subassembly with both prestressing and energy dissipaters can be evaluated by considering rigid body kinematics as shown in Figure 3 (c) and (d). Assume the neutral axis depth is small enough to be neglected and the horizontal force component from the threaded bolt bars is equal to the prestressing force in the bolt bars, joint equilibrium gives:

$$F_p = \left(P^-_{ps}\frac{e}{D} + P^+_{ps}\left(1-\frac{e}{D}\right)\right)\cos\alpha\frac{D}{L_{col}}\frac{L}{L_b} \quad \textbf{(4)}$$

where P^-_{ps} and P^+_{ps} are the total tendon force in the precast beam when rocking along the bottom and top edge, respectively; e = eccentricity of prestressing tendon at column face as shown in Figure 3, D = beam depth; L = bay length; L_b = precast beam length; and α = angle of the threaded fuse-bolt bars.

Similarly, when considering the influence of the dissipaters' yield capacity on the subassembly:

$$F_D = F_{diss\,y}\frac{D}{L_{col}}\frac{L}{L_b} \quad \textbf{(5)}$$

where $F_{diss\,y}$ = total yield force of the supplementary energy dissipaters.

The lateral strength at yielding of the subassembly is:

$$F_{p\,yield} = P_{ps\,yield}\cos\alpha\frac{D}{L_{col}}\frac{L}{L_b} \quad \textbf{(6)}$$

where $P_{ps\,yield}$ = yield strength of fuse bolt bars.

The prestressing force within the tendon at both ends can be expressed via the prestressing loss formula as:

$$\frac{P_2}{P_1} = e^{(-\mu_f\alpha_{ps}-\kappa l)} \quad \textbf{(7)}$$

where P_1 = force at jack end and P_2 = force at the anchor end, μ_f = angular coefficient of friction, α_{ps} = angle change of the tendon in radian unit, κ = wobble loss coefficient, and l = length of the tendon where prestress loss are considered.

Assuming the wobble loss (κl) is small and can be neglected, and the friction loss ($\mu\alpha$) values are also small so that its higher order terms in the expanded expression can be neglected, the prestress losses in the tendon after opening or closing of the gap (δF) can be derived as:

$$\delta F = \mu_f \alpha_{ps} P_1 \quad \textbf{(8)}$$

In a jointed precast frame, the large inelastic rotation is accommodated via gap opening and closing at the unbonded post-tensioned connections. At the ends of the member large concentrated forces are expected. According to St. Venant's principle, the high stress region behind the force will spread to approximately one section depth. This effect introduces additional member flexibility and reduces the effective stiffness of the beam-column joint. Using moment-area theorems, the effective stiffness of the precast member can be approximated as:

$$\psi = \frac{EI_{eff}}{EI_g} = \frac{1}{6\left(\frac{1}{\alpha_D{}^3\beta} - 1\right)\frac{D}{L_b}\left(1 - \frac{D}{L_b}\right) + 1} \quad \textbf{(9)}$$

where α_D = effective section depth ratio, and β = effective section width ratio. When unidirectional loading is applied to the subassembly, the precast beams will rock along the top and bottom edges of the steel armor plate, therefore β = 1 and α_D should take a small value close to zero, while for bi-directional loading the beams are expected to rock about a corner and hence β should also take a small value close to zero. Nevertheless, as will be explained in more detail later, the armored rocking interface in the tested subassembly showed some flexibility and did not perfectly rock about the edge and corner during the unidirectional and bi-directional tests, respectively. Hence, the values of these constants (α_D = 0.5 and β = 1 for unidirectional and α_D = 0.5 and β = 0.5 for bi-directional tests) were chosen to suit the experimental outcomes. Thus the effective stiffness for in-plane only (unidirectional) and bi-directional rocking according to Equation (9) are ψ = 26% and ψ = 14% of the gross stiffness, respectively.

Unidirectional test results

Only a summary of the test results is presented herein, and more detailed description and discussion of the test results can be found elsewhere (Li 2006). A selection of the unidirectional test results is presented in Figure 4. During the initial 0.25% peak drift cycle, the connections in the subassembly remained closed, whereas the connections were observed to open slightly at a column drift of 0.5%. At 1% drift level, a single tension crack initiated at an angle of approximately 45 degree from the edge of precast beams at the tip of the steel angles. This crack opened and closed as the connection opened and closed. At 2% column drift, a minor compression crack developed behind the steel armor causing some minor spalling of cover concrete. At 3% column drift, uniformly spaced flexural cracks developed along all the precast beams. When tested with supplementary energy dissipaters, tensile cracks were found to develop behind the energy dissipater anchor plates. As expected, yielding of the energy dissipaters occurred almost immediately after the connection opening and large energy dissipated through tension yielding of the energy dissipaters. However,

compression buckling of the supplementary energy dissipaters occurred as the joints closed. This became more pronounced with increasing drift amplitudes. No cracks were observed along the precast column in all unidirectional tests.

It is clear from results presented in Figure 4 (a) and (b) that instead of a bi-linear-elastic force-drift response a small flag shaped force-drift response was achieved. This suggests that as a result of internal friction between the prestressing bolt bars and the encasing PVC ducts the subassembly dissipated a small amount of energy during these unidirectional tests even without any supplementary energy dissipaters installed. The energy dissipated in this manner is quantified in the following section. Figure 4 also plots the theoretical behavior of the test subassembly as predicted by using the proposed Equation (1). It is clear from the plots that any change in the amount of energy dissipation of the connection during rocking that resulted from change in prestress level as well as yielding of the supplementary dissipaters and bolt bars are well captured by Equation (1).

Bi-directional tests results

When subjected to bidirectional loading up to the design drift level of 2%, the subassembly performed well. Minor compression cracks were observed adjacent to the steel armor plate. Cracks similar to those in the unidirectional tests were also found in the bi-directional tests. Full re-centering of the test subassembly was achieved upon load removal. When the supplementary energy dissipaters were added onto the subassembly, an increase in energy dissipation was observed. The energy dissipaters yielded at column drift level of 0.5%, soon after the connection opened, and the dissipaters buckled upon joint closure.

To further study the behavior of the subassembly, tests were performed under bi-directional cosine based four-leaf clover pattern up to 4% radial column drift. This level of drift can be considered to be in excess of the seismic demands imposed by a maximum considerable earthquake (MCE) that has 2% probability of occurrence in 50 years. Results of this series of experiments are presented in Figure 5. First the subassembly was tested with the prestress only and then the test was repeated with the external energy dissipater. As can be seen in Figure 5 (b), the hysteresis plots of the subassembly when tested with prestressing only under bi-directional loading show flag shaped loops, similar to those obtained under unidirectional loading. Inherent friction between different components of the prestressing system resulted in additional energy dissipation. It was noticed that a large friction around the bent coupler resulted in small steps in the force-displacement curve at low drift levels in all tests.

As the test proceeded towards a radial column drift of 4%, more cracks appeared and minor crushing of concrete was observed at each corner of the beams adjacent to the steel angle armoring. Noticeable rounding of the steel armor plate along the top and bottom edges could be seen after the tests. This was attributed to the bi-directional loading effects that result in very high point forces at the outer corner of the armor plates at the beam ends. Although the subassembly was tested up to column drift of 4% in a radial direction, no torsional cracks were observed, indicating that the beam did not twist. This subsequently infers that the designed shear keys at the connection provided good resistance against torsional moments during these tests.

The strain gauge readings in the threaded fuse “bolt-bars” showed that these bars yielded just before the column reached a radial drift of 4% and this resulted in a slight loss of prestressing in the subassembly. The fuse “bolt-bars” were re-stressed after each test to maintain the initial prestress level in the subassembly. Nevertheless, as can be seen in Figure 5 (b) the subassembly maintained the strength up to 4% drift level. The maximum (in-plane) lateral forces were found to be 140kN in the EW direction and 70kN in NS direction.

Energy dissipaters were later installed and the subassembly was retested, the results are plotted in Figure 5 (c). As is clear from Figure 4, the supplementary energy dissipaters increased both the hysteretic energy dissipation and the lateral strength of the subassembly. Yielding of the threaded "bolt-bars" also provided some additional energy dissipation but reduced the peak strength during the repeated loading cycles. Although the energy dissipaters used in the specimens were found to be effective otherwise, these dissipaters buckled as the specimen re-centered. Large friction generated around the bent couplers resulted in small steps in force-displacement curves at low drift levels, observed in all previous tests. A smoother transition in the prestressing conduit around the bent region would mitigate this problem.

In accordance with Equation (9), the effective beam stiffness was found to be about 16% of the gross stiffness. The beam effectively rocked about a small area around the corner point of the angles armoring the beam ends. This reduction of the contact area at the rocking interfaces during bi-directional loading evidently justifies the use of St. Venants' principle to model the apparent reduction in beam stiffness.

Hysteretic energy dissipation

This section considers hysteretic energy dissipation in terms of equivalent viscous damping, which is a useful way to model a nonlinear hysteretic system using displacement based design. Based on a general expression for equivalent viscous damping (Clough and Penzien 1993), Pekcan et al (1999) derived the equivalent hysteretic damping of a bi-linear structural system, which is given by:

$$\xi_{hy} = \frac{1}{4\pi}\frac{E_D}{E_{so}} = \frac{2}{\pi}\eta\frac{(1-\alpha_k)\left(1-\frac{1}{\mu_\Delta}\right)}{(1-\alpha_k+\mu_\Delta\alpha_k)} \qquad \textbf{(10)}$$

where μ_Δ = displacement ductility; α_k = ratio of final to initial stiffness; η = energy absorption efficiency factor defined as the ratio of the area enclosed in the actual hysteresis loop (E_D) to the area under the equivalent linear elastic hysteresis curve (E_{so}) as shown in Figure 6 (a). The energy efficiency factor defined in Equation (10) can be modified for the subassembly with prestress only to be $\eta_{ps} = \mu\alpha_{ps}$, which can be obtained by substituting $\delta F = \mu\alpha_{PS}F_{max}$ from Equation (8) in the expression shown in Figure 6 (b).

When supplementary energy dissipaters are added, the equivalent viscous damping of the subassembly can be found by further modifying the energy absorption efficiency factor to take into consideration the effect of both prestressing losses and the yielding of the energy dissipaters:

$$\eta_{diss+ps} = \frac{\mu_f\alpha_{ps} + \left(\frac{F_{y\,diss}}{F_{\max}}\right)}{1+\left(\frac{F_{y\,diss}}{F_{\max}}\right)} \qquad \textbf{(11)}$$

According to Pekcan et al (1999), typical value of η for well designed ductile reinforced concrete is 0.35-0.4. Assuming an angular coefficient of friction $\mu_f = 0.25$ for the thread-bars; α_{ps} = 0.35rad at the couplers, the energy absorption efficiency factors of the subassembly with prestressing alone is $\eta_{ps} = 8.75\%$. When an energy dissipater with a yield strength of $F_{y\,diss}$ = 53kN is added, assuming F_{max} = 400kN (i.e. yield strength of the "bolt-bar"), the total energy absorption efficiency factor increases to $\eta_{ps+diss} = 19\%$.

Using these results along with Equation (6) with $\alpha = 0$, the theoretical values of equivalent viscous damping are calculated and plotted for the prestress only and prestress plus supplemental energy dissipaters in Figure 6 (c) and (d), respectively. Also plotted in the graph are the observed equivalent viscous damping factors, as determined from the area enclosed by the hysteresis loops in the experiments. Although the levels of damping are small, particularly for the prestress only case, the approach seems to adequately model the effects of hysteretic energy absorption.

Discussion

Steel armor plates provided good protection against structural damage, however they were not rigid enough to prevent beam end to deform flexibly during rocking. This flexible-rocking or rolling-rocking action at the connection slightly reduced the initial stiffness of the subassembly as observed in Figure 4. One way to improve rocking of the subassembly is to reverse the steel angles at end of the beam and to recess the concrete surfaces back 2 or 3mm from the connection. This would allow the precast beam to rock discretely along the edge of the steel angle's flange.

The supplementary energy dissipaters used in this experiment were designed to be externally mounted on the beam adjacent to the column with the intent to facilitate rapid replacement following yielding/buckling. However, the same supplementary energy dissipater could be designed to fit internally within the beam-column joint. Although the supplementary energy dissipaters provided adequate energy absorption especially when in tension, due to compression buckling the effectiveness of the present externally mounted dissipaters was reduced on cycles following the previous peak displacement (Dhakal and Maekawa 2002).

Prestress force losses due to friction during gap opening and closing resulted in approximately 5% of equivalent viscous damping at column drift of 3%. This increased to more than 10% with the addition of supplemental energy dissipaters. The tapered shear key details provided between the beam ends and the column face provided satisfactory resistance against the imposed torsional moments that tends to twist the beam under bi-directional moments. The two bottom shear keys allow the precast beam to be supported without any additional propping. Such shear keys hence also help increase the construction speed.

Note that the specimen was designed based on the assumption that the point of inflection occurs at the mid-length of beams, which is true when the frame is subjected to seismic load only. This assumption ignores the effect of gravity load transferred to the beam by the monolithic floor. Moreover, the specimen was tested with a constant axial load (which was approximately 7% of the column capacity), which is not representative of the different levels of axial load across the height of multistory buildings; e.g. the axial force is likely to be significantly higher in lower stories. Also, the tests in this study are conducted using a 3D beam-column specimen without a floor slab and the behavior of a subassembly with a floor slab will be different. Further studies are required to explore more realistic behavior of 3D jointed beam-column-slab sub-assemblies.

Conclusions

Based on the experimental investigation described herein, the following conclusions are drawn:

1. A simple steel-armored rocking connection designed without any welded parts has been demonstrated to be feasible in protecting precast concrete elements against seismic induced damage. The subassembly performed well up to bi-axial column

drifts of 4%. Although some minor superficial damage was observed adjacent to the armoring at the beam-ends, the remainder of the beam and column remained intact.

2. From the bi-directional lateral loading test results, the apparent stiffness of the beams is found to be in the order of $EI_{eff} = 0.16EI_g$. This reduction can be explained from St. Venants' principle due to the effect of the high point forces concentrated at the beam end corners during rocking. Based on a rational analysis, a formula has been derived to estimate this reduction in stiffness. Until more robust values are established through further experimental investigation, this value of EI_{eff} may be used to design such systems.
3. Several potential detailing improvements are identified from this experimental study. These include: (a) reversing the steel angle at the connection and recess the concrete surface back to improve rocking to avoid a rolling effect; (b) a smoother transition in the vicinity of the cable duct can be achieved by draping the tendon rather than using a bent coupler; (c) prevent the threaded energy dissipaters from buckling by sleeving and grouting the fuse area; and (d) explore new types of energy dissipaters such as viscous and visco-elastic dampers that have either re-centering capability or can creep to maintain zero force when the joint is closed.

References

Arnold, D. M. (2004). "Development and Experimental Testing of a Seismic Damage Avoidance Designed Beam to Column Connection Utilizing Draped Unbonded Post-Tensioning." *Masters Thesis*, *Department of Civil Engineering, University of Canterbury*, Christchurch, New Zealand, 188 pp.

Bradley, B. A., Dhakal, R. P., Mander, J. B., and Li, L. (2008). "Experimental multi-level seismic performance assessment of 3D RC frame designed for damage avoidance." *Earthquake Engineering and Structural Dynamics*, 37(1), 1-20.

Bull, D., and Brunsdon, D. (1998). "Examples of Concrete Structural Design to the New Zealand Standard Code of Practice for the Design of Concrete Structures-NZS3101." *Cement and Concrete Association of New Zealand (CCANZ)*, Wellington, New Zealand, 318 pp.

Clough, R. W., and Penzien, J. (1993). "Dynamics of Structures - Second Edition." *McGraw Hill*, pp. 648.

Davies, M. N. (2004). "Seismic Damage Avoidance Design of Beam-Column Joints using Unbonded Post-Tensioning: Theory, Experiments and Design Example." *Masters Thesis, Department of civil Engineering, University of Canterbury*, Christchurch, New Zealand, 155 pp.

Dhakal, R. P., and Maekawa, K. (2002). "Modelling for post-yield buckling of reinforcement." *Journal of Structural Engineering*, ASCE, 128(9), 1139-1147.

Li, L. (2006). "Further experiments on damage avoidance design of beam-to-column joints." *ME Thesis, Department of Civil Engineering, University of Canterbury*, Christchurch, New Zealand. http://library.canterbury.ac.nz/etd/adt-NZCU20060828.153252

MacRae, G. A., and Priestley, M. J. N. (1994). "Precast Post-Tensioned Ungrouted Concrete Beam-Column Sub-assemblage Tests." *Report No. SSRP-94/10, Department of Applied Mechanics and Engineering Sciences, University of California at San Diego*, California, USA.

Mander, J. B., and Cheng, C. T. (1997). "Seismic Resistance of Bridge Piers Based on Damage Avoidance Design." *Technical Report NCEER-97-0014, Department of Civil, Structural and Environmental Engineering, State University of New York at Buffalo*, New York, USA.

Menegotto, M., and Pinto, P. E. (1973). “Method of analysis for cyclically loaded reinforced concrete plane frames including changes in geometry and non-elastic behavior of elements under combined normal force and bending.” *IABSE Symposium on the Resistance and Ultimate Deformability of Structures Acted on by Well-defined Repeated Loads*, Lisbon.
Pekcan, G., Mander, J. B., and Chen, S. S. (1999). “Fundamental considerations for the design of non-linear viscous dampers.” *Earthquake Engineering and Structural Dynamics*, 28(11), 1405-1425.
Priestley, M. J. N., Sritharan, S., Conley, J. R., and Pampanin, S. (1999). “Preliminary result and conclusions from the PRESSS five-storey precast concrete test building.” *PCI Journal*, 44(6), 43-67.
Standards New Zealand. (1995). “Concrete Structures Standard NZS 3101:1995: Part 1: Code and Part 2: Commentary.” *Standards New Zealand*, Wellington.
Stone, W. C., Cheok, G. S., and Stanton, J. F. (1995). “Performance of hybrid moment-resisting precast beam-column concrete connection subjected to cyclic loading.” *ACI Structural Journal*, 92(2), 229-249.

List of figures

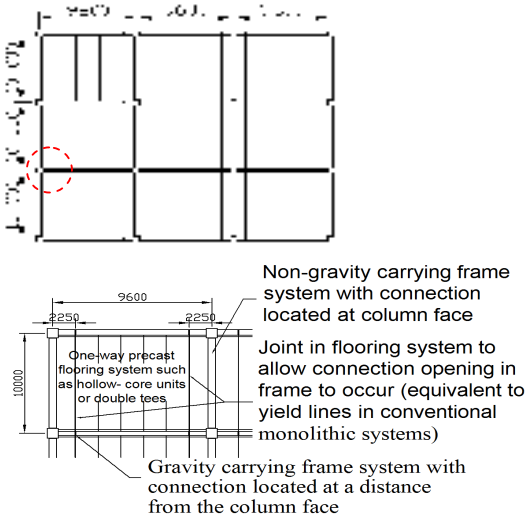

(a) Prototype building floor details.

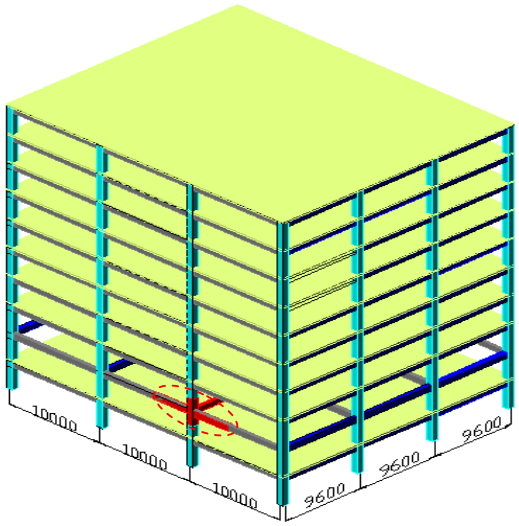

(b) Isometric view of the prototype building

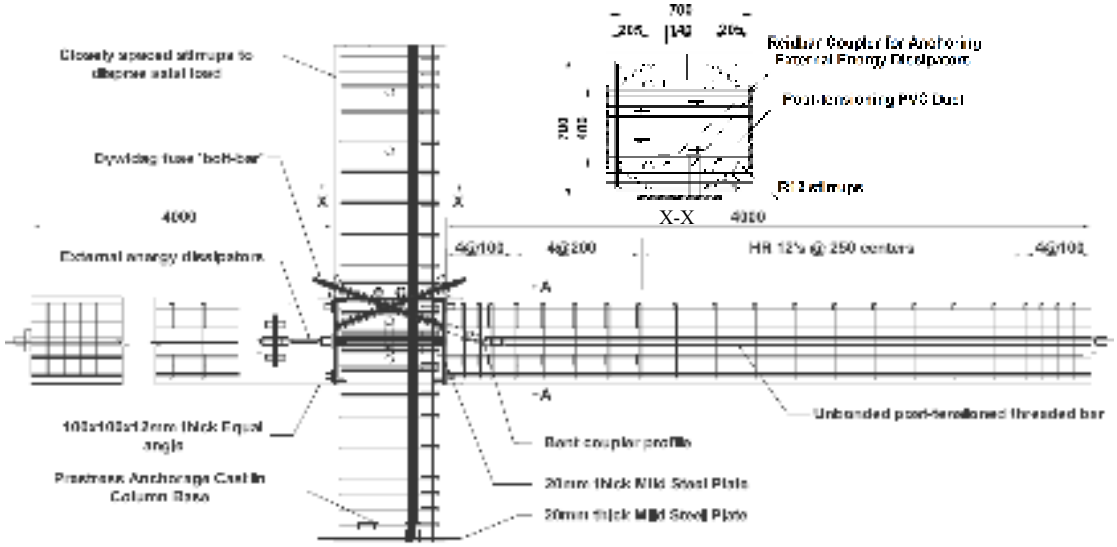

(c) Front (East-West) view of the test subassembly.

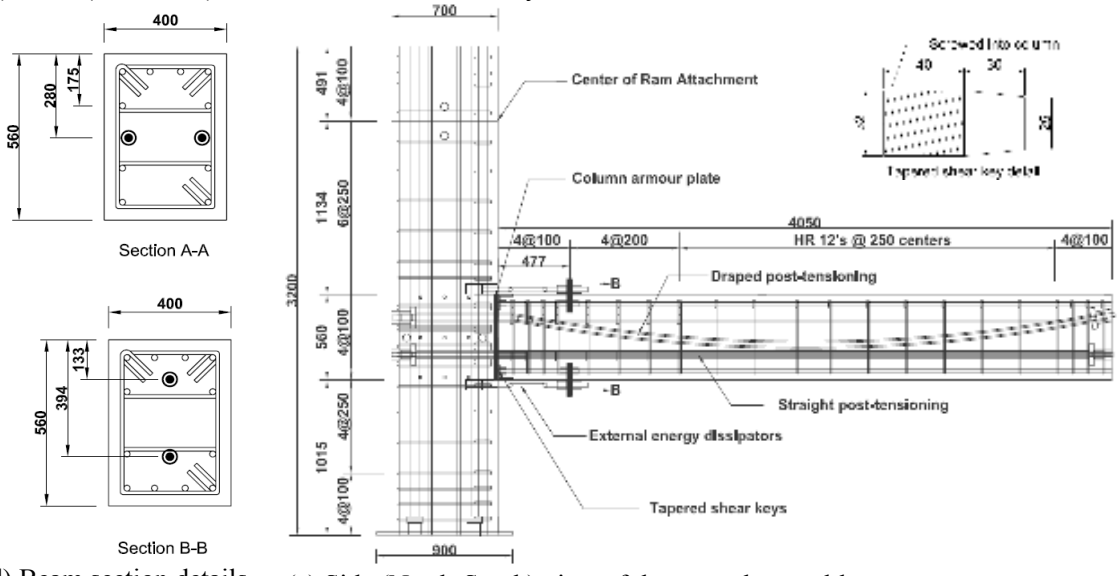

(d) Beam section details.

(e) Side (North-South) view of the test subassembly.

Figure 1: Prototype building and reinforcement details of the test subassembly.

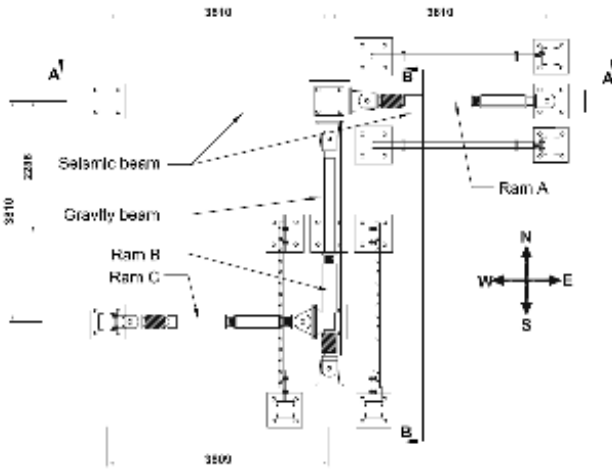

(a) Plan view.

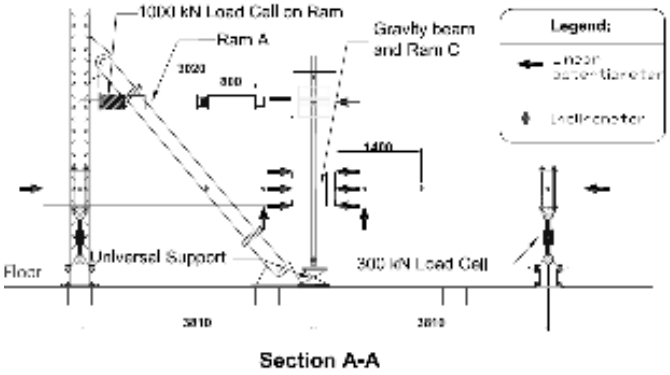

(b) Front view (Section A-A).

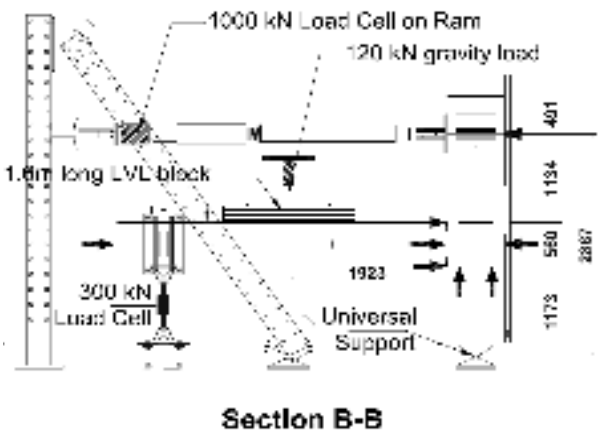

(c) Side view (Section B-B).

(d) Photograph of specimen.

Figure 2 Details of Experiment setup.

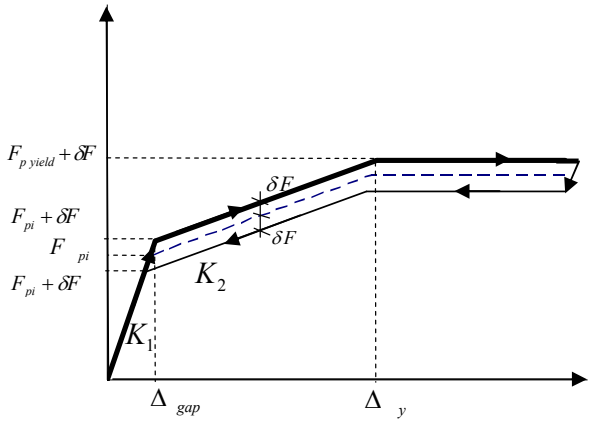

(a) Tri-linear response of the joint with prestress only.

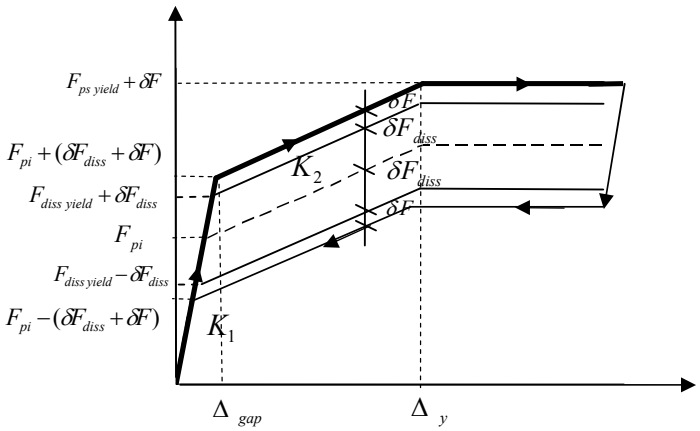

(b) Tri-linear response of the joint with prestress and external energy dissipaters.

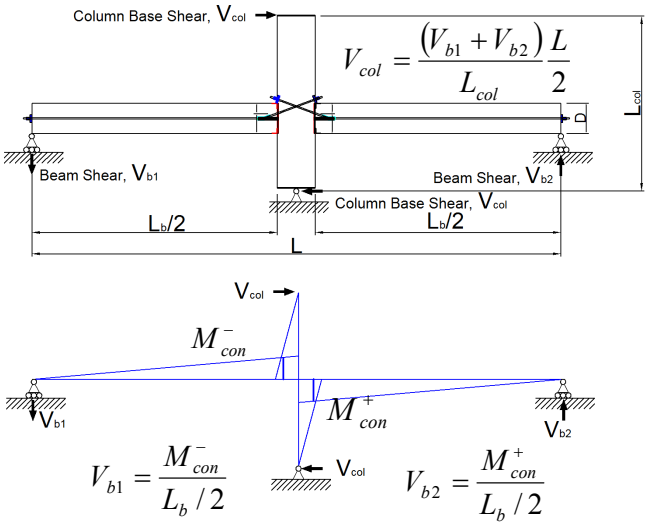

(c) Bending moment and reaction force of the joint.

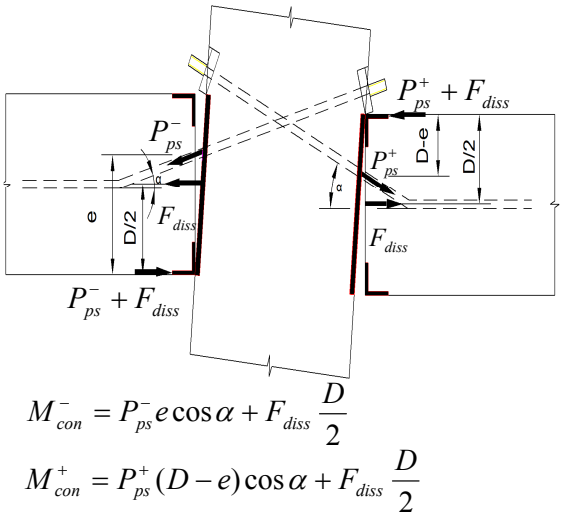

(d) Connection moment capacity of the joint.

Figure 3: Details of beam to column joint and bending moment diagram of the joint.

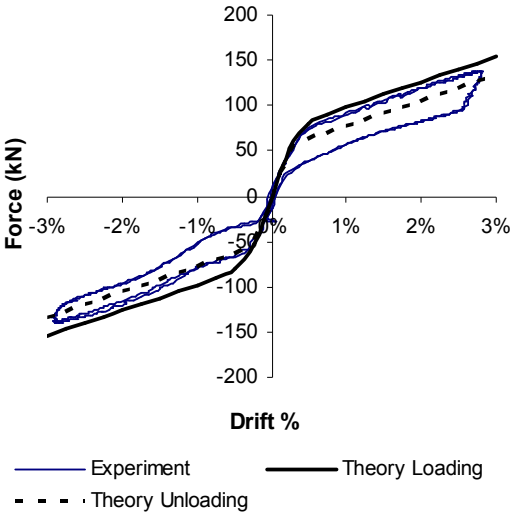

(a) E-W loading up to 3% lateral drift with initial prestressing force level of 50% of bar yield.

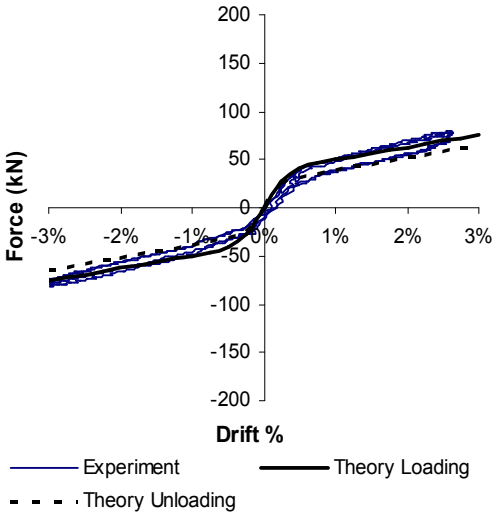

(b) N-S loading up to 2% lateral drift with initial prestressing force level of 50% of bar yield.

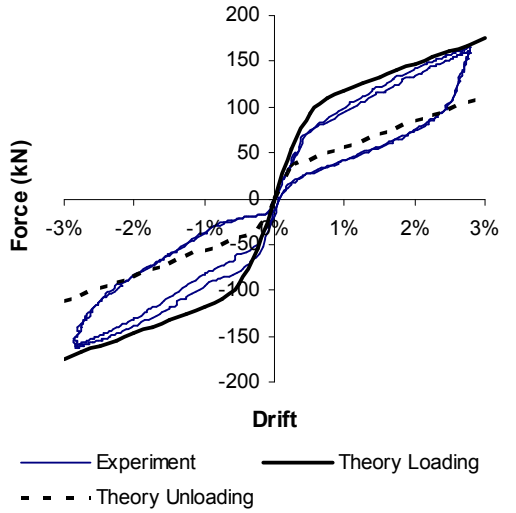

(c) E-W loading 3% lateral drift with threaded fuse rod dissipaters.

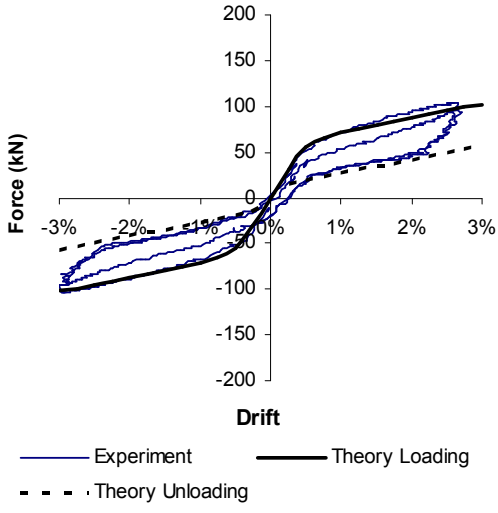

(d) N-S loading 3% drift with threaded fuse rod dissipaters.

Figure 4: Force-displacement response of subassembly tested under unidirectional loading to 3% lateral drift.

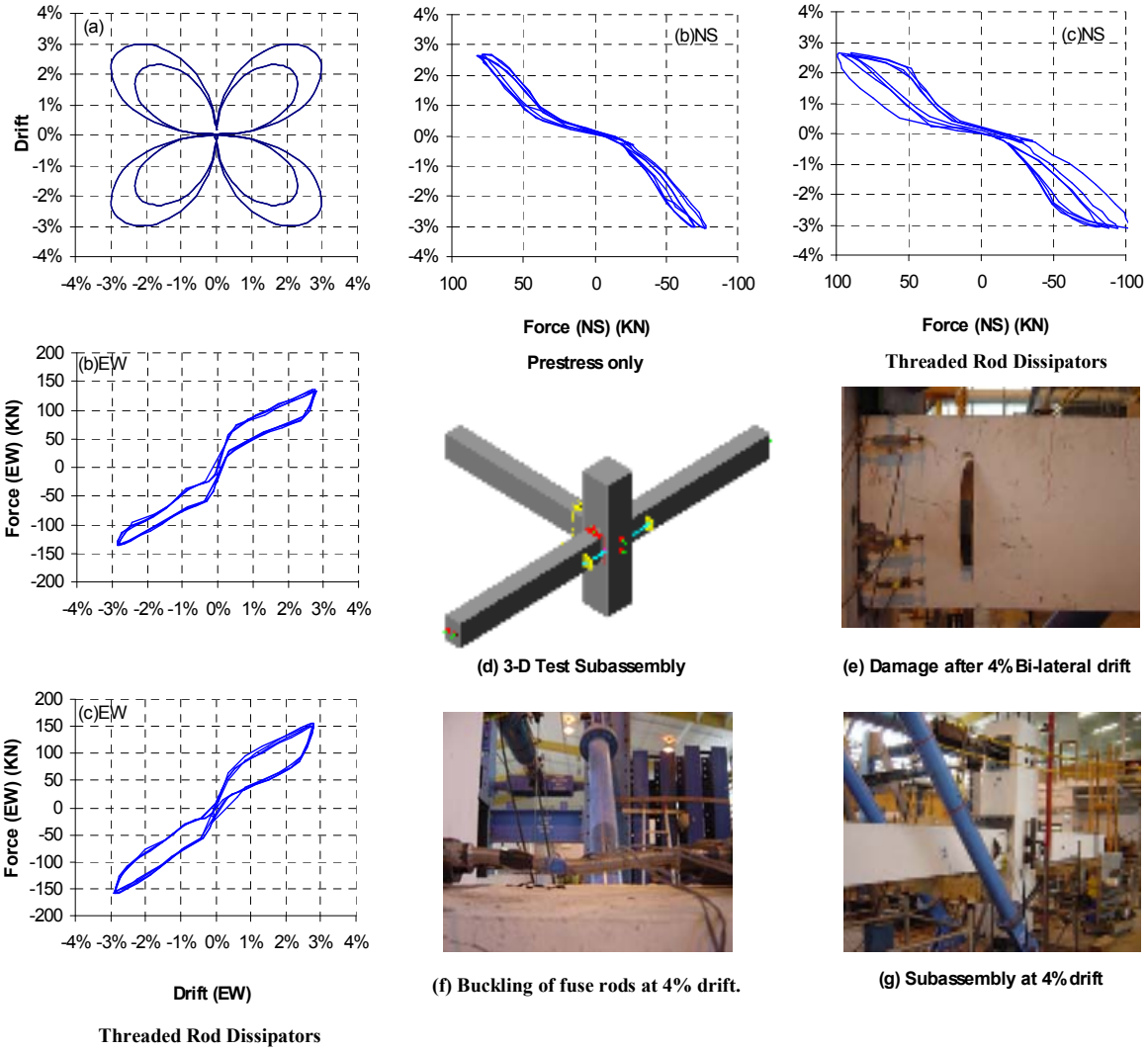

Figure 5: Experimental results of subassembly tested under bidirectional cosine-based 4-leaf clover pattern up to 4% radial drift showing: (a) Plan view of the bidirectional drift orbit; (b) Force-displacement plots of subassembly without dissipaters; (c) Force-displacement plots of subassembly with threaded rod dissipaters installed; (d) 3-D test subassembly; (e) Photograph of damage after 4% bi-lateral drift; (f) Photograph of buckled fuse rod at 4% drift; and (g) Test subassembly at 4% bi-lateral drift.

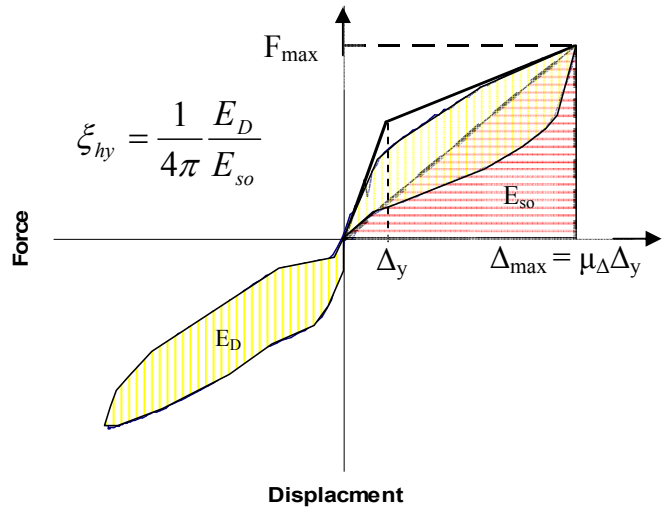

(a) Equivalent viscous damping based on energy consideration.

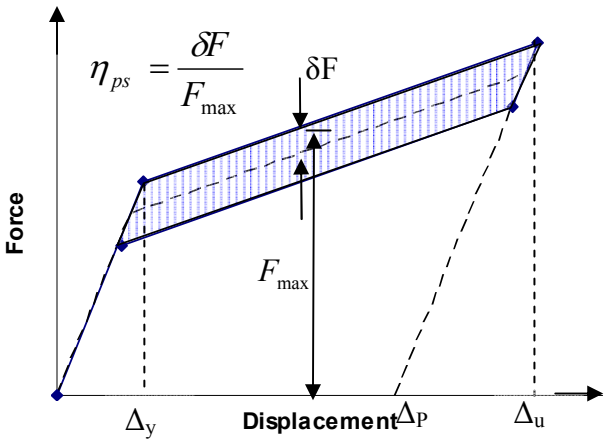

(b) Theoretical energy dissipation in the connection due to prestressing loss.

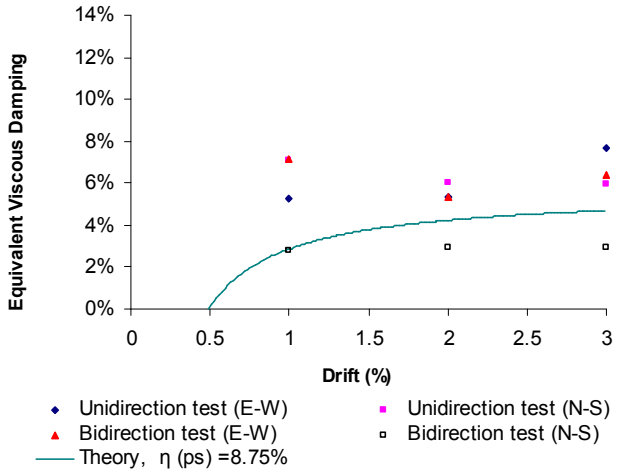

(c) Variation of equivalent damping in joint with prestress only.

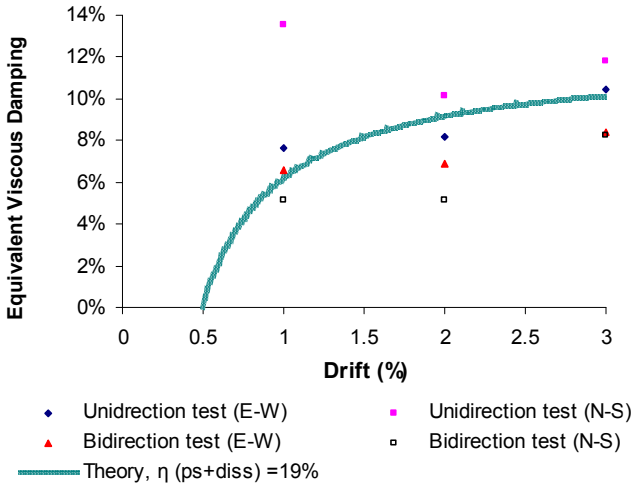

(d) Variation of equivalent damping in joint with prestress and supplementary energy dissipaters.

Figure 6: Equivalent viscous damping of the subassembly.